ФИЗИКА ЗЕМЛИ, 2010, № 8, с. 27–35

УДК 550.37

LARGE-SCALE THREE-DIMENSIONAL INVERSION OF EARTHSCOPE MT DATA USING THE INTEGRAL EQUATION METHOD

© 2010 г. Michael S. Zhdanov, Alisa Green, Alexander Gribenko, Martin Cuma

Department of Geology and Geophysics, University of Utah

Received January 25, 2010

In this paper we apply 3D inversion to MT data collected in the Northwestern United States as a part of the EarthScope project. By the end of 2009 MT data had been collected from 262 stations located throughout Oregon, Washington, Idaho, and most of Montana and Wyoming. We used data from 139 MT stations in this analysis. We developed fully parallelized rigorous 3D MT inversion software based on the integral equation method with variable background conductivity. We also implemented a receiver footprint approach which considerably reduced the computational resources needed to invert the large volumes of data covering vast areas. The data set used in the inversion was obtained through the Incorporated Research Institutions for Seismology (IRIS). The inversion domain was divided into 2.7 M cells. The inverted electrical conductivity distribution agrees reasonably well with geological features of the region.

INTRODUCTION

EarthScope is the United States Earth Science Program to explore the structure and evolution of the North American continent and understand processes controlling earthquakes and volcanoes. A major part of the EarthScope project is the Transportable Array which will be deployed over the next decade over the entire continental United States. This Transportable Array will provide an unparalleled means to study the geology of the United States. through seismology and other geophysical data. EMScope is the magnetotelluric component of the National Science Foundation's EarthScope USArray program. The MT Transportable Array comprises shorter-period investigations at hundreds of sites in the continental United States. By the end of 2009 MT data had been collected from 262 stations located throughout Oregon, Washington, Idaho, and most of Montana and Wyoming, 139 of which were used in this analysis (Fig. 1).

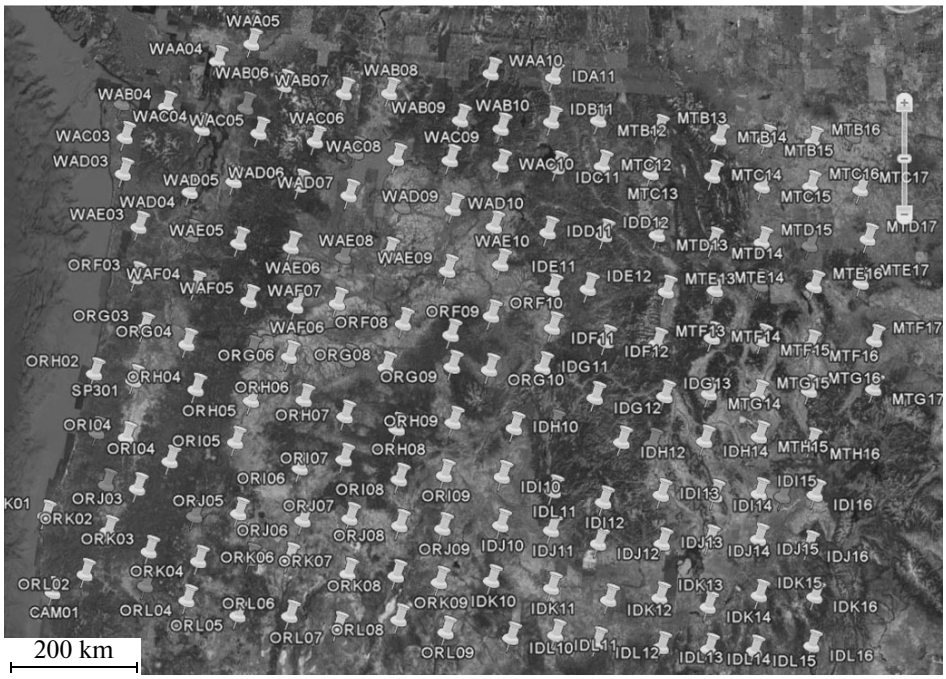

Fig. 1. The map of the Northwestern United States with the locations of the EarthScope MT stations shown by yellow pins.

The unique geological structure of the Northwestern United States is very important both for the study of its geodynamical history and for understanding the physical processes controlling earthquakes and volcanic eruptions [Bishop, 2003]. For such a complex region, definitive structural interpretations based purely on seismological observations may not be sufficient for reliable study of the deep earth interior. Conductivity in the subsurface plays a significant role in determining subsurface tectonic activities because of its sensitivity to temperature, the presence of interstitial fluids, melts, volatiles, and bulk composition. For example, many geological provinces merge in Oregon from the Columbia River basalts in the north to the Basin and Range in the south [Baldwin, 1981]. It is a tectonically active region with the subducting Juan de Fuca plate and volcanically interesting from the effects of the North American Plate traveling over the potential plume currently located beneath Yellowstone.

During recent years, magnetotelluric (MT) methods have experienced a rapid development. Significant improvements have been made both in MT data acquisition systems and in the quality of processing and analyzing this data. Modern MT surveys provide high quality data from an array of densely distributed MT stations, which contain unique information about the geoelectrical structure of geological formations. However, development of a truly three-dimensional (3D) inversion method still represents a very challenging numerical and practical problem. The reasons are twofold. First, 3D forward modeling is a highly complicated and time-consuming mathematical problem itself, especially for large-scale geoelectrical models. Second, the inversion of MT data is an unstable and nonunique problem. One should use regularization methods and physical constraints to obtain a stable and geologically meaningful solution of the inverse problem. There are several algorithms available now for 3D MT inversion. Some of these algorithms are based on rigorous forward modeling [Newman and Alumbaugh, 1997; Sasaki, 2004; Mackie and Watts, 2004; Siripunvaraporn 2005, Gribenko and Zhdanov, 2007; Zhdanov, 2009], while the others use approximate forward modeling operators [Zhdanov and Fang, 1996; Golubev et al., 1999; Zhdanov, 2000].

In this paper we introduce a method of rigorous 3D inversion of MT data, based on the integral equation (IE) method. We use the re-weighted regularized conjugate gradient method (RRCG) for nonlinear MT inversion [Zhdanov, 2002]. The main distinguishing feature of the RRCG algorithm is application of the special stabilization functionals which allow construction of both smooth images of the underground geoelectrical structures and models with sharp geoelectrical boundaries.

Besides the already complicated problem of nonlinear 3D EM inversion, there are computational difficulties associated with the vast inversion domains of regional MT surveys as well as the large amount of data. The so-called receiver "footprint" approach has been applied in airborne EM data inversion [Reid et al., 2006; Cox and Zhdanov, 2007] in an effort to reduce the computer resources required for 3D inversion of the real data sets. In this paper, we develop the footprint approach for MT data inversion. In the framework of this technique we use data from a receiver to recover conductivity structures only within a certain horizontal distance from this receiver. However, the entire anomalous domain is included in the computation of the predicted fields in the receivers. A footprint approach allows us to reduce dramatically computer memory requirements without loss of accuracy.

Another well known problem in 3D MT data inversion is the removal of static shift. The effect of static shift is due to the presence of small-scale, near-surface inhomogeneities. It manifests itself as a vertical shifting of the apparent resistivity curve by a frequency-independent factor, without any corresponding change in the phase curve. The amount of static shift varies from site to site, and differs depending on the source polarization. Thus, the interpretation of static-shifted MT data will obviously lead to erroneous results unless static shifts are correctly taken into account. Smith [1996] proposed static divergence correction for static shift. Another approach is to solve simultaneously for both resistivities and static shift parameters during 3D inversion [Sasaki, 2004]. We apply a static shift correction on the first stage of interpretation and then run 3D inversion of the corrected data.

In this paper we present the results of the 3D inversion of principal MT impedances from 139 MT stations collected at 28 frequencies ranging from 0.00006 to 0.3 Hz. As the forward modeling engine, we use the integral equation (IE) method [Hursán and Zhdanov, 2002]. We use the quasi-Born (QB) approximation for the Fréchet derivative calculation. This approximation is a reduction of the more general quasi-analytical approximation with variable background (QAVB) and possesses all of its qualities. QAVB is an effective and accurate technique for EM data inversion [Gribenko and Zhdanov, 2007; Zhdanov, 2009]. As a result of QB application, the IE-based method of MT inversion requires just one forward modeling in every iteration step, which results in a relatively fast but rigorous inversion method.

The major geoelectrical features recovered by the inversion agree well with the existing global geoelectrical models of the lithosphere. The 3D conductivity structures can be attributed to the specifics of the regional geology. Our inversion results show similar conductivity trends compared to other published works.

3D INVERSION OF THE MT DATA

IE method for 3D EM modeling

The integral equation (IE) method represents a powerful tool for electromagnetic (EM) numerical modeling and inversion [Weidelt, 1975; Hohmann, 1975; Wannamaker, 1991; Zhdanov, 2002; 2009]. This method is based on the reduction of the system of

Maxwell's equations to a system of integral equations with respect to the electric field within the inhomogeneity. The IE equation method can be effectively used for forward modeling the MT data.

Fig. 2 represents a sketch of a geoelectrical model used in the IE method. It is well known that the EM field in this model can be presented as a sum of the background (normal) $\{\mathbf{E}^b, \mathbf{H}^b\}$ and anomalous $\{\mathbf{E}^a, \mathbf{H}^a\}$ fields:

$$\mathbf{E} = \mathbf{E}^b + \mathbf{E}^a, \quad \mathbf{H} = \mathbf{H}^b + \mathbf{H}^a, \tag{1}$$

where the background field is a field generated by the given sources in the model with a background distribution of conductivity σ_b, and the anomalous field is produced by the anomalous conductivity distribution $\Delta\sigma\{r\}$, $r \in V \subset R^3$(see Fig. 2). Then, the electric and magnetic fields can be obtained by the following integral expressions:

$$\mathbf{E}(\mathbf{r}') = \iiint \mathbf{G}_E(\mathbf{r}', \mathbf{r})\Delta\sigma \boldsymbol{E}(\boldsymbol{r})d\nu + \boldsymbol{E}^b(\mathbf{r}'), \tag{2}$$

$$\mathbf{H}(\mathbf{r}') = \iiint \mathbf{G}_H(\mathbf{r}', \mathbf{r})\Delta\sigma \boldsymbol{E}(\boldsymbol{r})d\nu + \mathbf{H}^b(\mathbf{r}'), \tag{3}$$

where $r \in V \subset R^3$, and $\mathbf{G}_E$ and $\mathbf{G}_H$ are electric and magnetic Green's tensors.

These expressions become equations when $r' \in V$. A solution of each of these equations exists and is unique, as a solution of Fredholm equations of the second kind.

The process of solving the forward electromagnetic problem according to equations (2) and (3) consists of two parts. First, it is necessary to find the electric and magnetic fields inside the domain V (where $\Delta\sigma \neq 0$), which requires the solution of an integral equation (domain equation) (2) for $r' \in V$. Second, using the *data equations*, (2) and (3) with $r' \in P$, we calculate the EM field in the receiver domain P. Usually, the first part is more complicated and requires most of the computational time, because it consists of solving a large system of linear equations. We use a contraction form of the integral equation method [Hursán and Zhdanov, 2002; Zhdanov, 2009], which ensures a fast solution of the IE problem.

Magnetotelluric inverse problem

In MT methods, the earth's natural electromagnetic field is used as a source field. The mutually orthogonal horizontal components of electric and magnetic fields are recorded on the earth's surface. The interpretation of magnetotelluric data is based on the calculation of the transfer functions between the horizontal components of the electric and magnetic fields, which form the magnetotelluric impedance tensor [Berdichevsky and Dmitriev, 2002; 2008]:

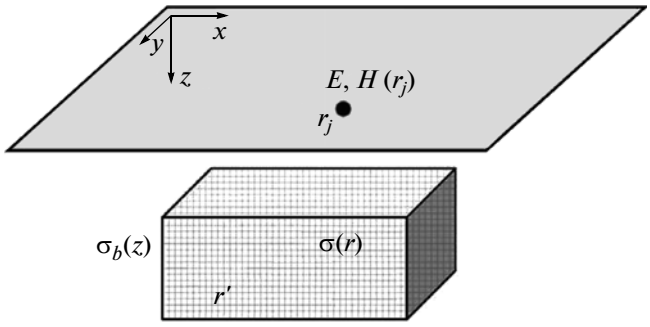

Fig. 2. Sketch of a geoelectrical model used in the IE method.

$$\hat{\mathbf{Z}} = \begin{bmatrix} Z_{xx} & Z_{xy} \\ Z_{yx} & Z_{yy} \end{bmatrix}. \tag{4}$$

The expressions for the components of the full impedance tensor are [Berdichevsky and Zhdanov, 1984]:

$$Z_{xx} = \frac{E_x^{(1)}H_y^{(2)} - E_x^{(2)}H_y^{(1)}}{H_x^{(1)}H_y^{(2)} - H_x^{(2)}H_y^{(1)}}, \quad Z_{xy} = \frac{E_x^{(1)}H_x^{(2)} - E_x^{(2)}H_x^{(1)}}{H_y^{(1)}H_x^{(2)} - H_y^{(2)}H_x^{(1)}}, \tag{5}$$

$$Z_{yx} = \frac{E_y^{(1)}H_x^{(2)} - E_y^{(2)}H_y^{(1)}}{H_x^{(1)}H_y^{(2)} - H_x^{(2)}H_y^{(1)}}, \quad Z_{yy} = \frac{E_y^{(1)}H_x^{(2)} - E_y^{(2)}H_x^{(1)}}{H_y^{(1)}H_x^{(2)} - H_y^{(2)}H_x^{(1)}}, \tag{6}$$

where $E^{(1)}$ and $H^{(1)}$ correspond to the nominal transverse magnetic (TM) mode, and $E^{(2)}$ and $H^{(2)}$ correspond to the nominal transverse electric (TE) mode. The concept of two modes of EM field (TM and TE modes) is widely used in MT. These ideas arose from one- and two-dimensional interpretation of MT data. In a 3D case we do not have true TE and/or TM modes. However, we can assume that in the nominal TE mode the direction of the electrical field $\mathbf{E}$ coincides with the direction of elongation of the anomalous structure in the Earth, while in the nominal TM mode those directions are perpendicular. For three-dimensional interpretation the TE and TM mode concept is used only as a convention.

We can describe the forward MT problem by an operator equation:

$$\mathbf{d}^{MT} = \mathbf{A}^{MT}(\Delta\sigma), \tag{7}$$

where $\mathbf{d}^{MT}$ stands for a *data vector* formed by the components of the MT impedance, and $\mathbf{A}^{MT}$ is the nonlinear forward operator symbolizing the governing equations of the MT modeling problem. We call equation (7) an *impedance equation*. The impedance equation is ill posed, i.e., the solution can be nonunique and unstable. The conventional way of solving ill-posed inverse problems, according to regularization

theory [Tikhonov and Arsenin, 1977; Zhdanov, 2002], is based on minimization of the Tikhonov parametric functional:

$$P^{MT}(\mathbf{m}) = \phi^{MT}(\mathbf{m}) + \alpha S(\mathbf{m}) = \min, \tag{8}$$

where $\phi^{MT}(\mathbf{m}) = \left\|\mathbf{A}^{MT}(\mathbf{m}) - \mathbf{d}^{MT}\right\|_2^2$ is the misfit functional between the predicted data $\mathbf{A}^{MT}(\mathbf{m})$ and the observed data $\mathbf{d}^{MT}$, $s(\mathbf{m})$ is a stabilizing functional, and α is a regularization parameter. The optimal value of α_{opt} is determined from the misfit condition,

$$\phi^{MT}(m_{\alpha_{\text{opt}}}) = \delta_d, \tag{9}$$

where δ_d is the noise level of the data.

The minimization problem (8) can be solved using any gradient-type technique. We use the re-weighted regularized conjugate-gradient (RRCG) method. Implementation details of this algorithm are specified in Zhdanov and Hursán (2000) and Zhdanov (2002).

MT Fréchet derivative calculation

In order to apply a gradient-type minimization technique, one need to be able to compute the Fréchet derivative of the forward operator $\mathbf{A}^{MT}$. Applying a variational operator to expressions (5) and (6), the following expression can be obtained:

$$\delta Z_{xy} = \sum_{i=1,2.} \left(\frac{\partial Z_{xy}}{\partial E_x^{(i)}} F_{E_x^{(i)}}[\delta\Delta\sigma] + \sum_{\alpha = x,y} \frac{\partial Z_{xy}}{\partial H_\alpha^{(i)}} F_{H_\alpha^{(i)}}[\delta\Delta\sigma] \right). \tag{10}$$

Here i means the mode, $i = 1$ for the TM mode, and $i = 2$ for the TE mode. Now the expressions for the partial derivatives of the impedance with respect to the field components, necessary for the computation of (10), take the following forms:

$$\frac{\partial Z_{xy}}{\partial E_x^{(1)}} = \frac{H_x^{(2)}}{H_y^{(1)}H_x^{(2)} - H_y^{(2)}H_x^{(1)}}, \tag{11}$$

$$\frac{\partial Z_{xy}}{\partial H_x^{(2)}} = \frac{H_x^{(1)}[E_x^{(2)}H_y^{(1)} - E_x^{(1)}H_y^{(2)}]}{[H_y^{(1)}H_x^{(2)} - H_y^{(2)}H_x^{(1)}]^2}, \tag{12}$$

$$\frac{\partial Z_{xy}}{\partial H_x^{(1)}} = \frac{H_x^{(2)}[E_x^{(1)}H_y^{(2)} - E_x^{(2)}H_y^{(1)}]}{[H_y^{(1)}H_x^{(2)} - H_y^{(2)}H_x^{(1)}]^2}, \tag{13}$$

$$\frac{\partial Z_{xy}}{\partial H_y^{(1)}} = \frac{H_x^{(2)}[E_x^{(2)}H_x^{(1)} - E_x^{(1)}H_x^{(2)}]}{[H_y^{(1)}H_x^{(2)} - H_y^{(2)}H_x^{(1)}]^2}, \tag{14}$$

$$\frac{\partial Z_{xy}}{\partial H_y^{(2)}} = \frac{H_x^{(1)}[E_x^{(1)}H_x^{(2)} - E_x^{(2)}H_x^{(1)}]}{[H_y^{(1)}H_x^{(2)} - H_y^{(2)}H_x^{(1)}]^2}, \tag{15}$$

$$\frac{\partial Z_{xy}}{\partial E_x^{(2)}} = -\frac{H_x^{(1)}}{H_y^{(1)}H_x^{(2)} - H_y^{(2)}H_x^{(1)}}. \tag{16}$$

The final expression for the Fréchet derivative of impedance tensor component Z_{xy} may be obtained by combining expressions (10)–(16) and taking into account the mode of the background field. The derivative of Z_{yx} with respect to $\Delta\sigma$ will take a similar form:

$$\delta Z_{yx} = \sum_{i=1,2} \left(\frac{\partial Z_{yx}}{\partial E_y^{(i)}} F_{E_y^{(i)}}[\delta\Delta\sigma] + \sum_{\alpha = x,y} \frac{\partial Z_{yx}}{\partial H_\alpha^{(i)}} F_{H_\alpha^{(i)}}[\delta\Delta\sigma] \right). \tag{17}$$

The following expressions describe the partial derivatives of the impedance with respect to the field components:

$$\frac{\partial Z_{yx}}{\partial E_y^{(1)}} = \frac{H_y^{(2)}}{H_x^{(1)}H_y^{(2)} - H_x^{(2)}H_y^{(1)}}, \tag{18}$$

$$\frac{\partial Z_{yx}}{\partial H_y^{(2)}} = \frac{H_y^{(1)}[E_y^{(2)}H_x^{(1)} - E_y^{(1)}H_x^{(2)}]}{[H_x^{(1)}H_y^{(2)} - H_x^{(2)}H_y^{(1)}]^2}, \tag{19}$$

$$\frac{\partial Z_{yx}}{\partial H_y^{(1)}} = \frac{H_y^{(2)}[E_y^{(1)}H_x^{(2)} - E_y^{(2)}H_x^{(1)}]}{[H_x^{(1)}H_y^{(2)} - H_x^{(2)}H_y^{(1)}]^2}, \tag{20}$$

$$\frac{\partial Z_{yx}}{\partial H_x^{(1)}} = \frac{H_y^{(2)}[E_y^{(2)}H_y^{(1)} - E_y^{(1)}H_y^{(2)}]}{[H_x^{(1)}H_y^{(2)} - H_x^{(2)}H_x^{(1)}]^2}, \tag{21}$$

$$\frac{\partial Z_{yx}}{\partial H_x^{(2)}} = \frac{H_y^{(1)}[E_y^{(1)}H_y^{(2)} - E_y^{(2)}H_y^{(1)}]}{[H_x^{(1)}H_y^{(2)} - H_x^{(2)}H_y^{(1)}]^2}, \tag{22}$$

$$\frac{\partial Z_{yx}}{\partial E_{xy}^{(2)}} = -\frac{H_y^{(1)}}{H_x^{(1)}H_y^{(2)} - H_x^{(2)}H_y^{(1)}}. \tag{23}$$

The final expression for the Fréchet derivative of impedance tensor component Z_{yx} may be obtained by combining expressions (17)–(23) and taking into account the corresponding mode of the background field. We show Fréchet derivatives for the Z_{xy} and Z_{yx}impedance components only, since they were used in the Oregon data inversion. The remaining derivatives can be obtained similarly.

In order to compute the Fréchet derivatives of the impedance components, we need to know Fréchet derivatives $F_E^{(i)}$ and $F_H^{(i)}$ of the field components themselves. We use the quasi-Born Fréchet derivative expressions to compute $F_E^{(i)}$ and $F_H^{(i)}$:

$$\mathbf{F}_{E,H}(\mathbf{r}_j|\mathbf{r}) = \iiint \hat{\mathbf{G}}(\mathbf{r}_j|\mathbf{r}) \cdot \mathbf{E}^{(n)}(\mathbf{r}) d\nu, \tag{24}$$

where $\hat{\mathbf{G}}_E(\mathbf{r}_j|\mathbf{r})$ and $\hat{\mathbf{G}}_H(\mathbf{r}_j|\mathbf{r})$ are the electric and magnetic Green's tensors defined for an unbounded conductive medium with a normal (horizontally layered) conductivity, domain D represents a volume with the anomalous conductivity distribution $\sigma(\mathbf{r}) = \sigma_{\text{norm}} + \Delta\sigma(\mathbf{r})$, and $\mathbf{r} \in D$. The domain electric field $\mathbf{E}^{(n)}$ is found at inversion iteration number n for the current conductivity model. Note that, the electric field $\mathbf{E}^{(n)}$ is computed, using the rigorous IE forward modeling

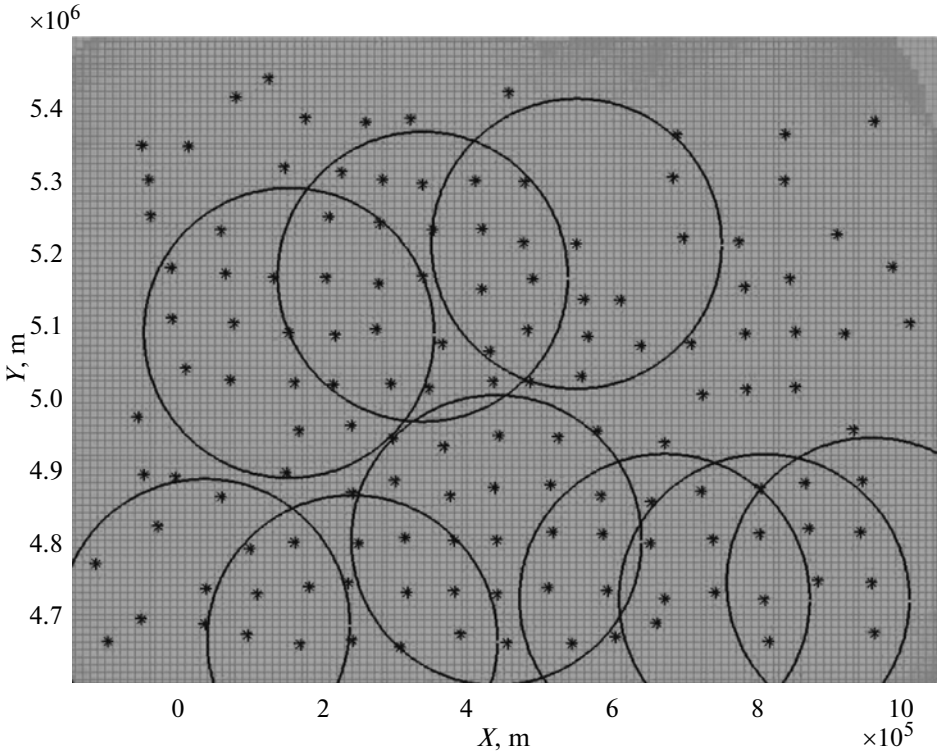

Fig. 3. A plan view of the location of MT stations with corresponding footprints. The stars show the positions of the stations. As an example, the footprint boundaries for several MT stations are shown by the black circles. The bright red color shows the area of overlap of the footprints for several closely located MT stations. One can see that in this case we have a complete continuous coverage of the entire area of observation with the overlapping footprints.

method. This field has to be found anyway in order to compute the predicted field in the receivers at each inversion iteration. Therefore, no extra computation is required to find the background field for the Fréchet derivative calculation.

The Fréchet derivative is the most expensive item in the inversion not only in terms of the computation time, but also in the computer memory required for its storage. The number of entries in the Fréchet derivative matrix is equal to the number of data points times the number of cells in the inversion domain. With large amounts of data and vast inversion regions, the computer memory requirements may become prohibitive. To reduce the storage requirements, we introduce the footprint approach in our MT inversion. In the framework of the footprint approach for a given receiver, we compute and store the Fréchet derivative inside the inversion cells only within a predetermined horizontal distance from this receiver. Fig. 3 shows a plan view of the location of the MT stations (receivers) with the corresponding footprints. The footprint area for every receiver is shown by a semitransparent red circle. The radius of the footprint was selected based on the rate of the corresponding Green's tensor attenuation. The bright red color shows the area of the overlap of the footprints for several closely located MT stations. The computer memory requirements are reduced dramatically by using the receiver footprint approach. Another advantage of this method is that the conductivities of the inversion cells are affected by the more dependable data from the nearby receivers only. Note that the entire domain of inversion is accounted for in the predicted field computations, thus keeping the 3D inversion accurate.

INTERPRETATION OF THE EARTHSCOPE MT DATA

Static shift correction

In the first stage of the interpretation, the EarthScope MT data set was corrected for static shift. The low frequency MT data can be adversely affected by near-surface conductivity anomalies, which leads to erroneous interpretation [Smith, 1996]. We developed a simplistic method for static shift correction, which is however very efficient in practical applications. The method is based on several assumptions. We assume that the static shift is random and is close to zero on average for all of the receivers (MT stations) and polarizations. Another assumption is that the regional horizontally layered one-dimensional (1D) earth structure changes slowly at great depths. Keeping these in mind, we inverted low frequency data for both the Z_{xy} and Z_{yx} components from all of the 139 available MT stations to recover a common 1D model. We used frequencies between 0.0001 and 0.00001 Hz, which approximately correspond to skin depths be-

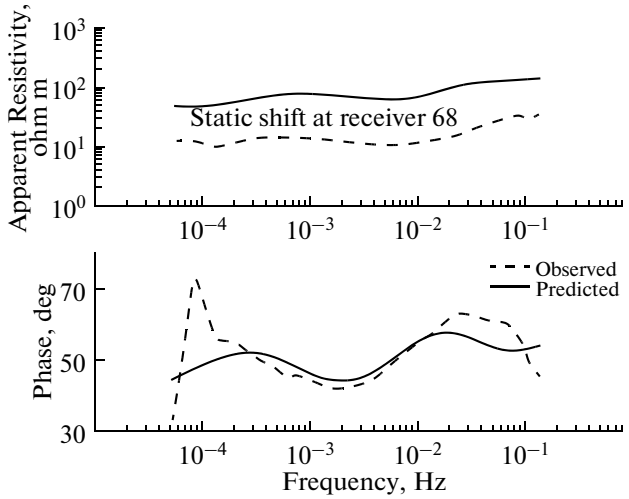

Fig. 4. An example of the observed and predicted apparent resistivity and phase curves after low frequency 1D inversion.

tween 150 and 400 km. We assumed that the discrepancies between the observed and predicted apparent resistivity curves at these frequencies were caused by the static shift primarily. The static shift was then computed as the ratio of the observed and predicted apparent resistivity curves. These ratios were averaged over nine frequencies used in 1D inversion.

Fig. 4 shows the plots of the observed and predicted TE apparent resistivity and phase for the receiver 16. One can see that the phase data fits well, while there is almost constant static shift between the observed and predicted apparent resistivity curves.

In order to check the proposed method of static shift correction, we performed 1D inversion on data from each receiver and polarization separately. We plotted the results of separate 1D inversions in 2D east-west and north-south profiles, combining several receivers. Fig. 5, left panel, shows an example of the south-north profile of TE and TM data inversion results for 11 receivers, including receiver #68. We corrected this data for static shift using the technique de-

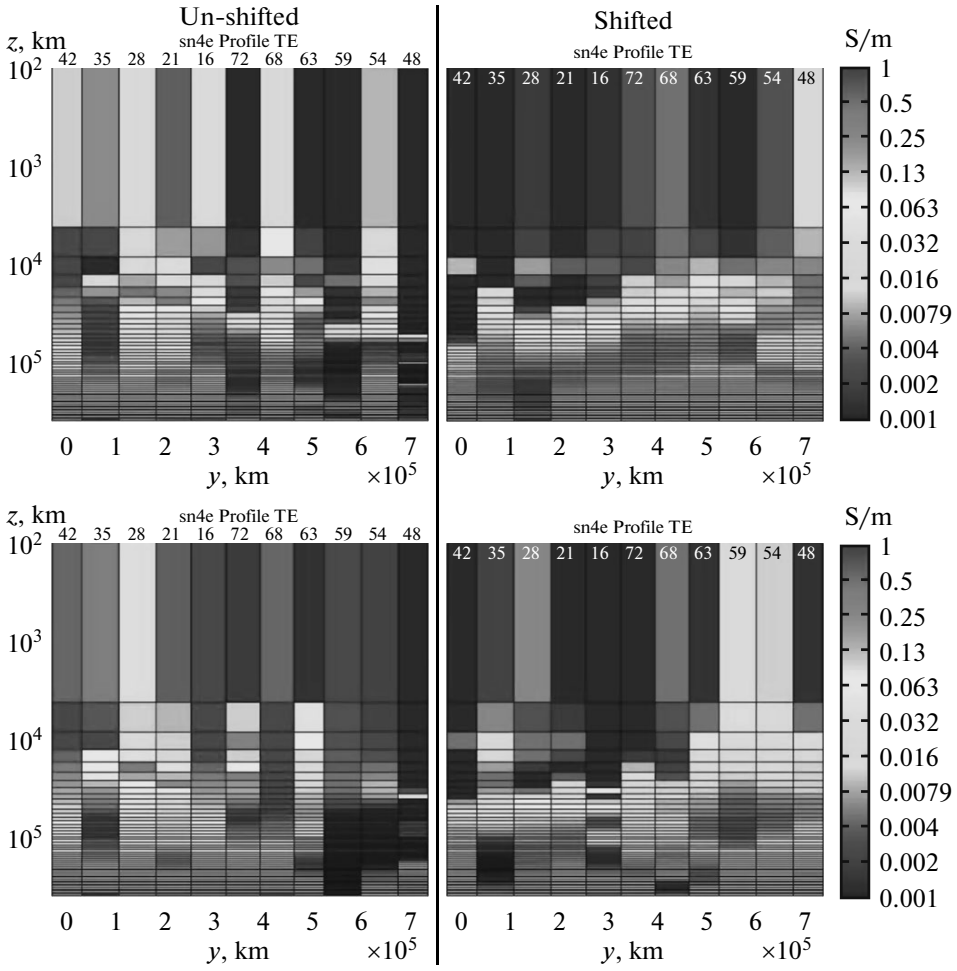

Fig. 5. The images on the left show 1D inversion results for a south-to-north profile prior to static shift correction. The images on the right show 1D inversion results for the same south-to-north profile after static shift correction. Station numbers are shown at the top.

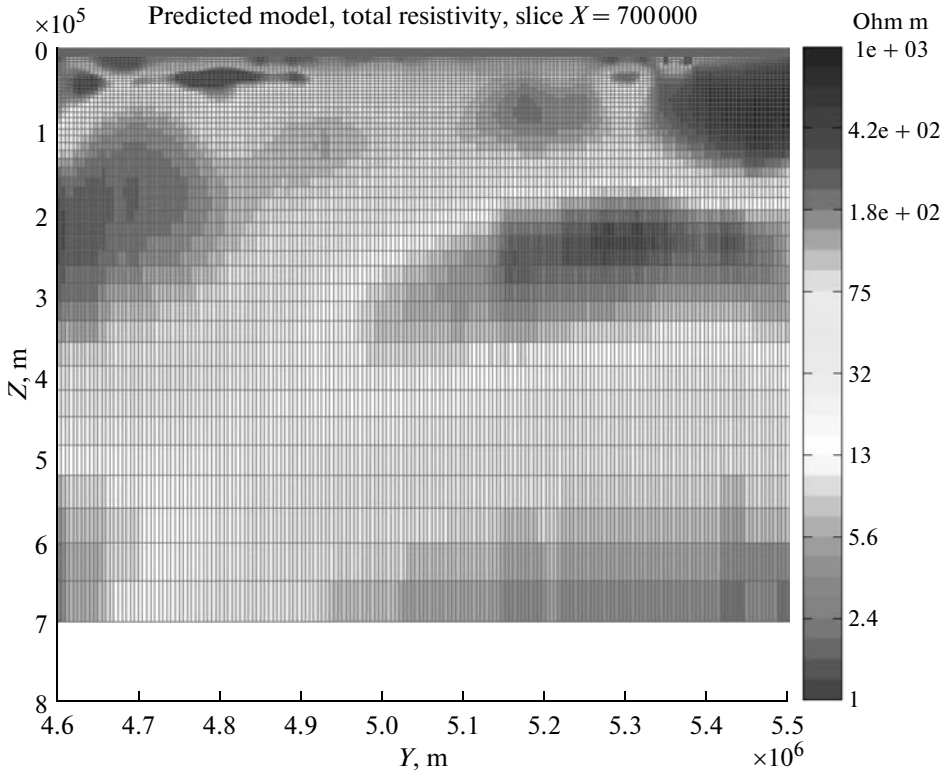

Fig. 6. A north-south vertical resistivity section at $X = 700$ km through the inverse geoelectrical model.

scribed above, and re-run 1D inversion for receiver 68, using corrected data. Fig. 5, right panel, shows the same south- north profile, as above, after the static shift correction. Note that, after static shift corrections, the 1D inversion result for receiver 68 shows resistivities in the same range as in the other receivers. This example demonstrates that the proposed technique for static shift correction can be effectively applied to EarthScope MT data.

Analysis of the results of 3D inversion

After completing a static shift correction, we applied our 3D IE based inversion to the Z_{xy} and Z_{yx} data from all 139 receivers at 12 frequencies distributed logarithmically between 0.05 and 0.0002 Hz. Fig. 3 shows the positions of the MT stations (the receivers). The inversion domain is spanned in the X and Y directions from –150 to 1050 km, and from 4600 to 5500 km, respectively. The depth of the inversion domain was selected at 700 km. We used discretization cells with a horizontal size of 5 km by 5 km, and vertical cell sizes ranging from 0.5 km at the top of the inversion domain to 50 km at the very bottom, increasing with depth logarithmically. The total number of cells in the inversion domain was around 2,764,800. The initial model was selected as an 80 Ohm m half-space. Inversion was run for 28 smooth iterations, and the normalized misfit decreased from 27% to 8%.

We present here, as an example, a vertical section of the inversion. Fig. 6 represents a north-south vertical resistivity section at $X = 700$ km through the inverse geoelectrical model. We attribute the most visible conductive anomaly at depths between 200–300 km to the conductive astenosphere. The thickness of the astenosphere is overestimated because of low vertical resolution of low frequency data. We can see that the astenosphere appears shallower and more conductive in the northern part of the profile. Another conductive anomaly is visible at a depth of approximately 50 km, and can be attributed to the conductive lower crust [Jones, 1999].

Fig. 7 shows a 3D geoelectrical model obtained by the inversion of the EarthScope MT data in the form of combined vertical resistivity sections. The geoelectrical model of the Northwestern U.S. deep interior produced by 3D inversion indicates several electrical conductivity anomalies in the lithosphere including a linear zone marked by low-to-high conductivity transition along the Klamath Blue Mountain Lineament associated with a linear trend of gravity minima. High electrical conductivity values occur in the upper crust under the accreted terrains in the Blue Mountains region.

Fig. 8 represents a 3D view of a geoelectrical model obtained by inversion of the EarthScope MT data with a conductive astenosphere shown as a massive 3D structure. Note in conclusion, that our inverse model correlates well with the published Patro and Egbert (2008) results obtained for EarthScope data collected in the state of Oregon only.

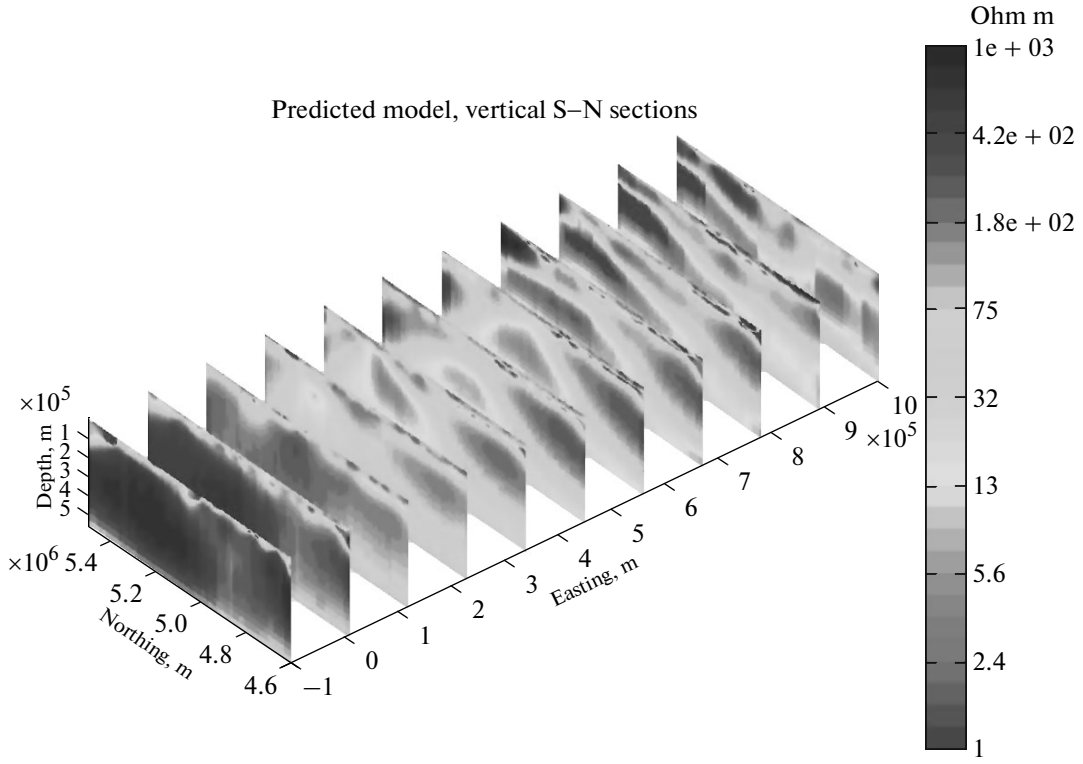

Fig. 7. A 3D geoelectrical model obtained by the inversion of EarthScope MT data in the form of vertical resistivity sections.

Conclusions and future research

We have applied a 3D MT inversion algorithm to the MT data from 139 Northwestern U.S. MT stations available through the EarthScope project. The observed data were corrected for static shift using a newly developed method based on 1D low-frequency data inversion. Our study demonstrates that the integral equation based inversion method can be successfully applied to real data sets on a regional scale with large data volume. The geoelectrical model obtained as a result of this inversion correlates reasonably well with the available seismic information.

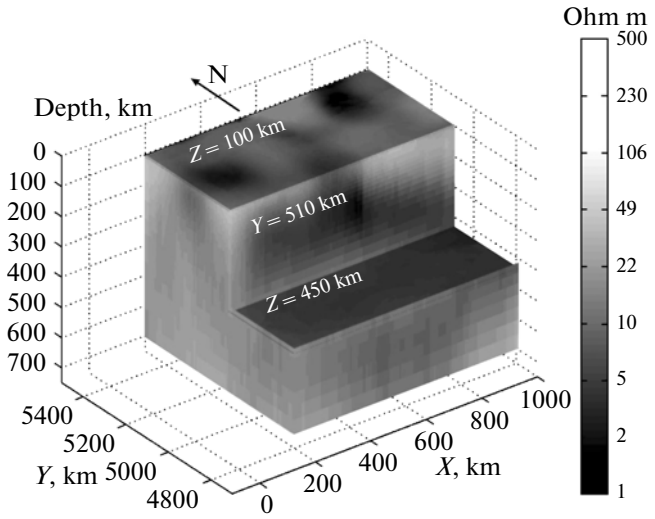

Fig. 8. 3D view of the resistivity model obtained from the inversion of EarthScope MT data with a conductive astenosphere shown.

The scope for joint 3D inversion of both seismic and MT data offers the opportunity to improve geological interpretations developed by either method alone. Such 3D interpretation requires fast and accurate methods of modeling large-scale problems. A family of 3D MT modeling algorithms has been developed by the CEMI consortium based on integral equation and finite-difference methods. The codes have been partially adapted for parallel computing and are available for large-scale modeling and interpretation of regional-scale MT data observations. Though the joint inversion of seismic and MT data are currently not available, such a project would provide a very interesting avenue for future research.

The authors acknowledges the support of the University of Utah Consortium for Electromagnetic Modeling and Inversion (CEMI), which includes BAE Systems, Baker Atlas Logging Services, BGP China National Petroleum Corporation, BHP Billiton World Exploration Inc., BP, EMGS, ENI S.p.A., ExxonMobil Upstream Research Company, Fugro, Halliburton Energy Services, Information Systems Laboratories, Newmont Mining Co., OHM, Petrobras, PGS, Rio Tinto - Kennecott, Rocksource, Russian Research Center Kurchatov Institute, Schlumberger, Science Applications International Co., Shell International Exploration and Production Inc., StatoilHydro, Sumitomo Metal Mining Co., Total, Woodside Energy, and Zonge Engineering and Research Organization.

We also acknowledge allocation of computer time provided by the University of Utah's Center for High Performance Computing (CHPC).

Data used in this study were made available through Earth-Scope (www.earthscope.org; EAR-0323309), supported by the National Science Foundation.

REFERENCES

Baldwin E.M. Geology of Oregon: Edward Bothers, Inc. 1964 and 1981.

Berdichevsky M.N., Zhdanov M.S. Advanced theory of deep geomagnetic sounding: Elsevier. 1984.

Berdichevsky M.N., Dmitriev V.I. Magnetotellurics in the context of theory of ill-posed problems: Society of Exploration Geophysicists, Tulsa, OK. 2002. 215 p.

Berdichevsky M.N., Dmitriev V.I. Models and methods of magnetotellurics: Springer-Verlag, Berlin, Heidelberg. 2008. 563 p.

Bishop E.M. In search of ancient Oregon: A geological and natural history: Timber Press. 2003.

Cox L., Zhdanov M.S. Large scale 3D inversion of HEM data using a moving footprint: 78th Annual International Meeting, SEG, Expanded Abstracts. 2007. P. 467–471.

Golubev N.G., Zhdanov M.S., Matsuo K., Negi T. Three-dimensional inversion of magnetotelluric data over Minami-Noshiro oil field: Proceedings of the Second International Symposium of Three-Dimensional Electromagnetics, University of Utah. 1999. P. 305–308.

Gribenko A., Zhdanov M.S. Rigorous 3D inversion of marine CSEM data based on the integral equation method // Geophysics. 2007. V. 72. P. 229–254.

James D.E., Fouch M.J. High Lava Plains Seismic Experiment. Presented at the Burns Town Meeting. 2006.

Jones A.G. Imaging the continental upper mantle using electromagnetic methods: Lithos. 1999. V. 48. P. 57–80.

Hohmann G.W. Three-dimensional induced polarization and EM modeling // Geophysics. 1975. V. 40. P. 309–324.

Hursán G., Zhdanov M.S. Contraction integral equation method in three-dimensional electromagnetic modeling: Radio Science. 2002. V. 37. P. 1089–2002.

Mackie R.L., Watts M.D. The use of 3D magnetotelluric inversion for exploration in complex geologic environments; potential pitfalls and real world examples: Eos, Transactions, American Geophysical Union. 2004. V. 85. GP14A-01.

Newman G.A., Alumbaugh D.L. Three-dimensional massively parallel inversion – I. Theory: Geophysical Journal International. 1997. V. 128. P. 355–363.

Patro P.K., Egbert G.D. Regional conductivity structure of Cascadia: Preliminary results from 3D inversion of USArray transportable array magnetotelluric data. Geophysical Research Letters. 2008. V. 35. L20311, doi:10.1029/2008GL035326.

Reid J.E., Pfaffling A., Vrbancich J. Airborne electromagnetic footprints in 1D Earths // Geophysics. 2006. V. 71. 2. G63–G72.

Roth J.B., Fouch M.J., James D.E., Carlson R.W. 3D seismic velocity structure of the northwestern United States // Geophysical Research Letters. 2008. 35. 12 p.

Sasaki Y. Three-dimensional inversion of static-shifted magnetotelluric data // Earth Planets Space. 2004. V. 56. P. 239–248.

Siripunvaraporn W., Egbert G., Lenbury Y., Uyeshima M. Three-dimensional magnetotelluric inversion; data-space method // Physics of the Earth and Planetary Interiors. 2005. V. 150. P. 3–14.

Smith J.T. Conservative modeling of 3-D electromagnetic fields, Part II: Biconjugate gradient solution and an accelerator // Geophysics. 1996. V. 61. P. 1319–1324.

Tikhonov A.N., Arsenin V.Y. Solution of ill-posed problems / V.H. Winston and Sons. 1977.

Wannamaker P.E. Advances in three-dimensional magnetotelluric modeling using integral equations // Geophysics. 1991. V. 56. P. 1716–1728.

Weidelt P. EM induction in three-dimensional structures // Geophysics. 1975. V. 41. P. 85–109.

Zhdanov M.S., Fang S. 3D quasi-linear electromagnetic inversion: Radio Science.1996. V. 31. P. 741–754.

Zhdanov M.S.., Fang S., Hursán G. Electromagnetic inversion using quasi-linear approximation // Geophysics. 2000. V. 65. P. 1501–1513.

Zhdanov M.S., Hursán G. 3D electromagnetic inversion based on quasi-analytical approximation // Inverse Problems. 2000. V. 16. P. 1297–1322.

Zhdanov M.S. Geophysical inverse theory and regularization problems. Amsterdam, New-York, Tokio: Elsevier. 2002. 609 p.

Zhdanov M.S. Geophysical electromagnetic theory and methods. Amsterdam, New-York, Tokio: Elsevier. 2009. 848 p.